Langmuir

Article

pubs.acs.org/Langmuir

Porous Silicon/Photosynthetic Reaction Center Hybrid Nanostructure

Kata Hajdu,[†] Csilla Gergely,*[,§,∥] Marta Martin,[§,∥] Thierry Cloitre,[§,∥] László Zimányi,[⊥] Katalin Tenger,[⊥] Petro Khoroshyy,[⊥] Gabriela Palestino,[#] Vivechana Agarwal,[▽] Klára Hernádi,[‡] Zoltán Németh,[‡] and László Nagy[†]

Departments of [†]Medical Physics and Informatics and [‡]Applied and Environmental Chemistry, University of Szeged, Szeged, Hungary

[§]Université Montpellier 2 and [∥]CNRS, Laboratoire Charles Coulomb UMR 5221, Montpellier, France

[⊥]Institute of Biophysics, Biological Research Centre of the Hungarian Academy of Sciences, Szeged, Hungary

[#]Facultad de Ciencias Químicas, Universidad Autónoma de San Luis Potosí, San Luis Potosí, Mexico

[▽]CIICAP - Universidad Autonoma del Estado de Morelos, Cuernavaca, Mexico

ABSTRACT: The purified photosynthetic reaction center protein (RC) from *Rhodobacter sphaeroides* R-26 purple bacteria was bound to porous silicon microcavities (PSiMc) either through silane-glutaraldehyde (GTA) chemistry or via a noncovalent peptide cross-linker. The characteristic resonance mode in the microcavity reflectivity spectrum red shifted by several nanometers upon RC binding, indicating the protein infiltration into the porous silicon (PSi) photonic structure. Flash photolysis experiments confirmed the photochemical activity of RC after its binding to the solid substrate. The kinetic components of the intraprotein charge recombination were considerably faster (τ_{fast} = 14 (±9) ms, τ_{slow} = 230 (±28) ms with the RC bound through the GTA cross-linker and only τ_{fast} = 27 (±3) ms through peptide coating) than in solution (τ_{fast} = 120 (±3) ms, τ_{slow} = 1387 (±2) ms), indicating the effect of the PSi surface on the light-induced electron transfer in the protein. The PSi/RC complex was found to oxidize the externally added electron donor, mammalian cytochrome *c*, and the cytochrome oxidation was blocked by the competitive RC inhibitor, terbutryne. This fact indicates that the specific surface binding sites on the PSi-bound RC are still accessible to external cofactors and an electronic interaction with redox components in the aqueous environment is possible. This new type of biophotonic material is considered to be an excellent model for new generation applications at the interface of silicon-based electronics and biological redox systems designed by nature.

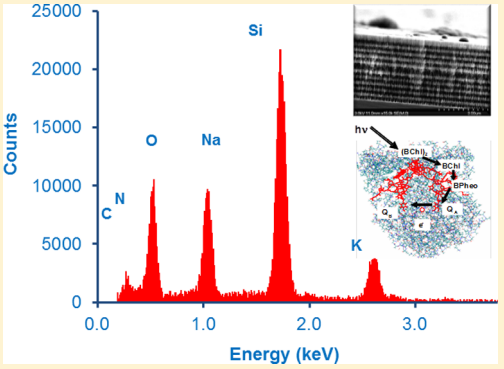

INTRODUCTION

The application of technical developments in biology (e.g., actuators, artificial tissues, and drug delivery systems) and vice versa, i.e., biological materials in technical developments (e.g., environmentally friendly biodegradable items and biosensor devices) are the focus of current research and industrial interest.[1−3] The use of biological materials developed by nature to perform extremely efficient and sensitive functions, with exceptional capacity, would be beneficial in (bio)hybrid systems. Among these systems, the bionanocomposites are of special interest because of their combined advantageous properties and the possibility of the appearance of some new characteristics. There are many potential applications of bionanocomposite materials such as biosensors, integrated (opto)electronic devices (switches or converters), photoelectric energy conversion, and (single-molecule) imaging.[2,4]

To fabricate bionanocomposite substances, one of the most promising materials is silicon because of its abundance and wide application in semiconductor technology.[5] However, light-sensitive biomolecules as the biological components are promising because of their extremely fast performance and efficient energy conversion.[6,7] In a successful combination of silicon-based materials and light-sensitive biological molecules (e.g., light-energy-converting proteins), a bionanocomposite can be designed to convert light energy efficiently within a tunable time (from femtoseconds to seconds) and wavelength range (from UV to IR).

Different types of silicon and silica-based substances have been described in the literature for hosting photosynthetic materials (at any level of organization from whole cells to molecules) either as a passive environment for assuring proper conditions for biological structure and function or as an active component participating in biological functions (charge separation and stabilization). The encapsulation of whole plant cells into various silica-based matrices is a promising target for the development of sustainable technology such as bioreactors.[8] Mesoporous silica materials (MPS) have been shown to successfully retain the structure and function of the photosynthetic reaction center protein in FSM (folded-sheet mesoporous silica material) and SBA-15 (Santa Barbara Amorphous porous silica material) and those of the light-harvesting pigment protein complex (LHC), which is another

Received: May 8, 2012
Revised: July 16, 2012
Published: July 19, 2012

transmembrane component of the photosynthetic apparatus.[9−12]

In recent years, PSi has emerged as a promising material for photonic applications, sensors, and novel drug delivery methods.[13−20] Various applications of PSi in bionanotechnology are due to its (a) possible integration with the IC technology, (b) tunable pore dimensions, (c) large surface area, (d) fabrication of fine multilayered photonic structures, (e) easy, cheap fabrication method, and (f) biodegradable nature. Because of their exceptional electrical and optical properties, the PSi multilayered photonic structures offer unique application possibilities in integrated optoelectronic and biosensing (biophotonic) devices as well.[17,18,21,22]

The application of photoactive pigment protein complexes in PSi-based biophotonic devices is a new challenge. RCs are integrated pigment−protein complexes in the photosynthetic membranes of plant and bacterial cells and constitute the site where the primary steps of the photoelectric energy conversion take place during photosynthesis. The capture of light energy by bacteriochlorophylls in photosynthetic bacteria results in the separation of positive and negative charges in the P^+BPheo^- state followed by the $P^+Q_A^-$ state, where P^+ is the oxidized primary electron donor, a specialized bacteriochlorophyll dimer, $(BChl)_2$; BPheo is the first electron acceptor, a monomer bacteriopheophytin; and Q_A^- is the reduced quinone-type primary electron acceptor. The separated charges are then further stabilized in the form of the $P^+Q_B^-$ redox state, where Q_B^- is the reduced secondary quinone.[23−25]

Our group has already investigated the possible unique applications of the RC protein in nanostructures or in optoelectronic systems (e.g., as fast optical switches, biosensors, and imaging or energy-converting systems[26,27]). Some of the special properties of RCs allowing such applications are the following: (a) Characteristic absorption and absorption transitions in the near-infrared (700−1000 nm) provide a unique possibility for the potential application of the RC in optoelectronic systems as a detector because this is beyond the visible range but does not require the complicated technology necessary in the far IR. (b) During and after light excitation, there are kinetic transitions with different lifetimes inside the protein (from the excitation in a few femtoseconds to the primary charge separation in picoseconds followed by charge recombination lasting for seconds). By site-directed mutagenesis, the RC protein can be modified to generate a redox process and absorption transitions in almost any desired time domain. This possibility can be advantageous, for example, in optical switches working in time domains of several orders of magnitude. (c) The photosynthetic reaction centers are nature's best "energy converting devices"; the quantum efficiency of the primary charge separation is almost 100%.[7] (d) The redox centers appearing inside the protein after excitation can interact with their environment (either on the electron donor or on the acceptor side), and the resulting redox systems can potentially be utilized in numerous applications,[3,28] for instance, in circuit segments of electrochemical cells.

In this work, the incorporation of RCs (size of about 10 nm diameter) into the PSi photonic structures has been shown after binding them covalently through functionalized groups or noncovalently through a high-affinity peptide coating.[29,30] Flash photolysis experiments demonstrate the retention of the photochemical activity (in single/multiple turnover) of the protein adsorbed on the PSi. Such hybrid structures offer the possibility of utilizing RCs as a light-activated transient electronic interface between the silicon substrate and redox partners in the bulk solution.

RESULTS AND DISCUSSION

Morphological Characterization of the PSiMc before and after RC Binding. To confirm the presence of RC within the PSiMc, elemental compositional analysis by energy-dispersive X-ray spectroscopy (EDX) was performed over the whole cross section of the untreated (Figure 1) and modified

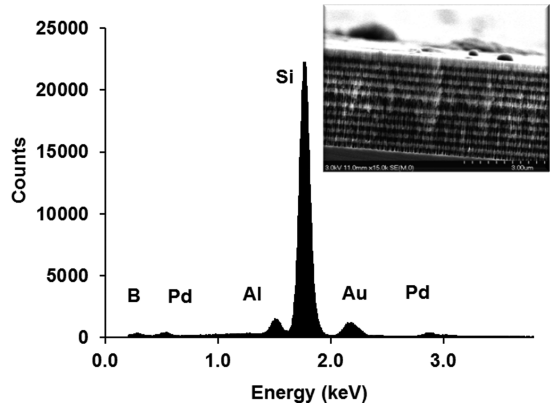

Figure 1. Result of the element analysis by energy-dispersive X-ray spectroscopy for untreated PSiMc. The elements corresponding to the peaks are indicated. The inset shows the SEM image of the multilayer structure of bare PSiMc.

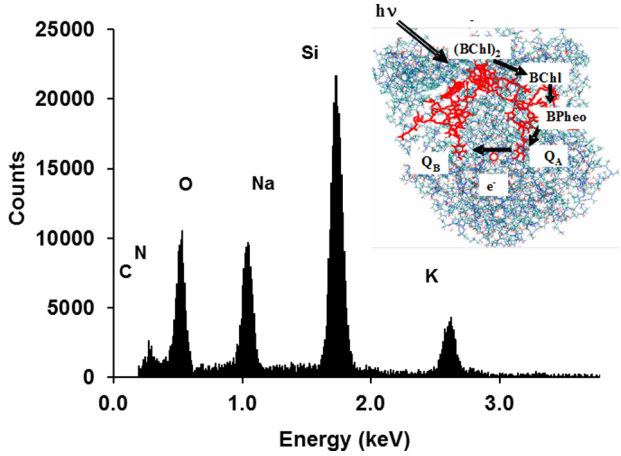

Figure 2. Result of the element analysis by energy-dispersive X-ray spectroscopy for PSiMc treated with 6.0 μM RC. The elements corresponding to the peaks are indicated. The inset shows the protein frame and the redox-active cofactors of the photosynthetic reaction center. $(BChl)_2$: primary electron donor bacteriochlorophyll dimer. BChl: bacteriochlorophyll monomer. BPheo: bacteriopheophytine. Q_A and Q_B are the primary and secondary quinone-type electron acceptors, respectively. Black arrows represent the electron-transport route along the cofactors.

(Figure 2) photonic structure. In the untreated PSiMc, the EDX spectrum showed the abundance of Si (Figure 1). In Figure 2, RC-treated samples display significant amounts of C, N, and O due to the presence of the protein. Signals of elements such as Au, Pd, and Al originated from the sample prepreparation phase (sputtering and sample holders). In the

dx.doi.org/10.1021/la301888p | Langmuir 2012, 28, 11866−11873

cross-sectional SEM image, a well-defined, multilayered porous structure, symmetric with respect to the thick active layer, is clearly visible, in good agreement with the literature (inset in Figure 1).[13,31]

Optical Monitoring of RC Incorporation into PSiMc Structures. The characteristic optical response of PSiMc used to monitor the immobilization efficiency of biomolecules within the porous structure is the shift of a well-defined photonic resonance dip in the stop band of the reflectivity spectrum. Specular reflectometry monitors the reflected energy from the sample surface at a given angle of incidence. The electromagnetic and physical phenomena that occur at and below the surface are dependent upon the angle of incidence of the illumination beam, the refractive index modulation, and the thickness of the porous multilayer. The narrow resonance peak (cavity mode) is very sensitive to the change in refractive index that is caused by molecular infiltration.

Figure 3 shows that after APTES and GTA binding the resonance peak of PSiMc structures shifts slightly to the red,

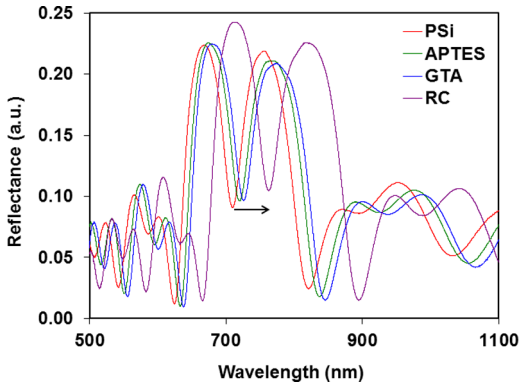

Figure 3. Reflectance spectra of the PSiMc recorded at different steps in the chemical treatment of the sample. Incubation of the chemically pretreated PSiMc was done at a saturating RC concentration of 6 μM. The arrow indicates the red shift induced by the RC binding. PSi: untreated PSiMc sample. APTES, GTA, and RC: subsequent treatments.

but after RC binding, a more pronounced red shift is observed. The relative enhancement in the magnitude of the red shift after RC binding can be attributed to the increased change in the effective refractive index of the nanostructured photonic structure, which, in turn, is related to the quantity of the protein captured by the device. The red shift is found to depend on the protein concentration in the incubation medium.

Although the RC is a naturally asymmetric protein in terms of charge and hydrophobicity, the chemical (APTES-GTA)-functionalization protocol that we follow assures its binding to PSi with a random orientation because the RC can be bound to PSi by any amine group presented by the protein. Less is known about the details (i.e., orientation preference) of the affinity-type binding via the specific peptide. The protocol also eliminates the unbound RC fraction or RCs bound nonspecifically in the last step of washing with PBS buffer containing TX-100 detergent. The role of electrostatic interactions in the binding affinity of the water-soluble glucose oxidase (GOX) is discussed in detail by Palestino et al.[18] Similar to GOX, the net surface charge of the RC at pH 8.0 is very negative[32] (pI of the RC is 6.1), resulting in an effective repulsive force between the PSi surface and the protein. Because RC is a trans-membrane protein, a large part of its surface is hydrophobic, which does not favor electrostatic binding to the PSi either.

The optical response of the functionalized PSiMc samples was evaluated by the dose response curves of the devices shown in Figure 4. Binding of the RC to PSiMc can be modeled by

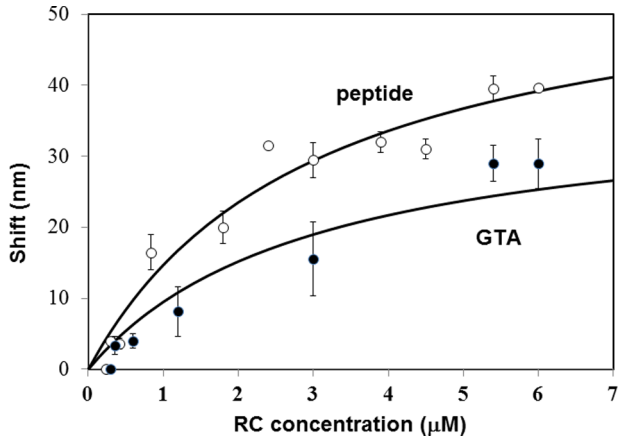

Figure 4. Magnitude of the red shift of the resonance peak as a function of the incubation concentration of the RC. PSiMc was functionalized with either GTA after silanization (●) or a specific peptide coating with the sequence SPGLSLVSHMQT (○) as described in the text. Solid lines were calculated by the equation: $\Delta\lambda_c = \Delta\lambda_{max}[RC]/([RC] + K)$. Here $\Delta\lambda_c$, $\Delta\lambda_{max}$, and K are the red shift at the given RC concentration, the expected maximum shift, and the RC concentration at $\Delta\lambda_{max}/2$, respectively. The values of r^2 for the fit were 0.95 and 0.9 for the peptide and the GTA samples, respectively.

standard single-saturation kinetics: $\Delta\lambda_c = \Delta\lambda_{max}[RC]/([RC] + K)$. Here $\Delta\lambda_c$, $\Delta\lambda_{max}$, and K are the red shift at the given RC concentration, the expected maximum shift, and the RC concentration at $\Delta\lambda_{max}/2$, respectively. The fitted parameters are $\Delta\lambda_{max} = 59(\pm5)$ and $38(\pm8)$ nm and the concentrations at $\Delta\lambda_{max}/2 = 3.0$ (±0.6) and 2.8 (±1.5) μM for the peptide and for the GTA methods, respectively. These parameters strongly suggest that the peptide linker offers better conditions for the integration of the bacterial reaction centers into the PSiMc structure compared to those obtained with the PSiMc modified via silane-GTA chemistry.

Furthermore, the standard deviations are smaller and the curve obtained with the peptide method runs above that obtained with the GTA cross-linker at any RC concentration (i.e. at same concentration of RC, the red shift was always larger in the case of the peptide method than with the GTA one). Because the affinity (K) of RC toward the two types of surfaces is roughly the same, this phenomenon may be attributed to the higher density of RC binding sites on the peptide-coated surface than on the silanized samples with the GTA cross-linker, favoring nonspecific binding over the chemical one. The larger red shift in the resonance peak for the peptide method correlates with the larger number of active RCs bound to the surface as shown by the functional assay (see later).

Though the mechanism of peptide−molecule binding is not clear yet, previous studies demonstrated that the modification of Si via the Si-specific SPGLSLVSHMQT peptide provides better interface layers for molecular binding and the peptide coating generates a more homogeneous and hydrophobic surface, hence the RC can also bind to the surface quite

homogeneously.[17] It was found earlier that the high hydrophobicity of membrane proteins seems to be an important factor for better adsorption and functional characteristics in nanopores of FSM, which is probably the case in PSi as well.[10] Moreover, the peptide layer provides an ideal interface for preventing the denaturation of biomolecules during adsorption, as demonstrated earlier.[33] Maintaining the RC activity after immobilization on PSi is crucial for an active, functional hybrid material.

RC Activity Assay: Single Turnover. Without an externally added electron donor, the RC performs a single turnover after light excitation and a pair of positive (P^+) and negative (Q_A^- or Q_B^-) charges is formed within the protein. The RC can be excited again only when it is reset by charge recombination. To test the RC activity with immobilization on the surface of PSiMc, time-resolved flash-induced absorption change measurements were carried out in a reflection arrangement at 860 nm (Figure 5A). Assuming that the

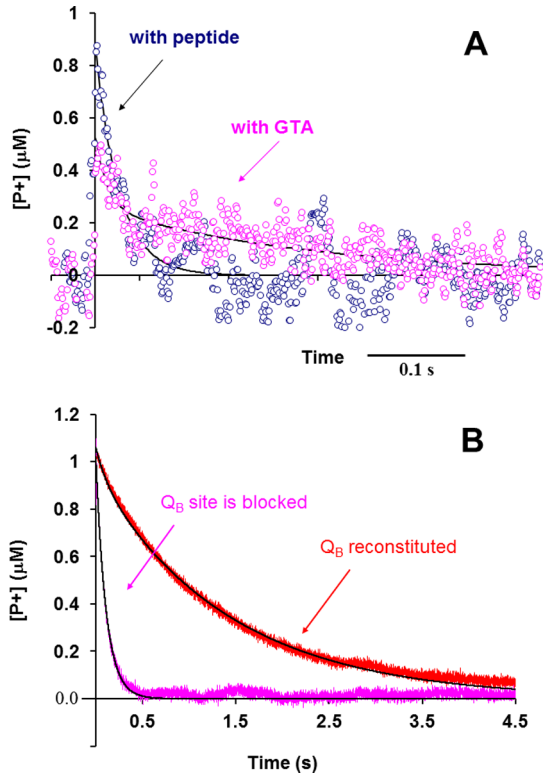

Figure 5. Amount of the oxidized primary donor, P^+, of the RC bound to PSiMc (A) or in buffer solution (B) as obtained from the 860 nm absorption change in the dark relaxation phase after a single saturating light excitation. (A) RCs were bound to PSiMc through GTA cross-linkers or the specific peptide, as indicated. Solid lines are the (bi)exponential fits with the parameters summarized in Table 1. (B) RCs were fully reconstituted by 100 μM UQ-0 (Q_B sample), or the Q_B site was blocked by the specific inhibitor, terbutryne (Q_A sample). The buffer contained 10 mM TRIS, 100 mM NaCl, and 0.03% LDAO (pH 8.0).

differential extinction coefficient at 860 nm for RC bound to PSi is the same as measured in solution (128 $mM^{-1}cm^{-1}$),[34] we can estimate the amount of RC bound to PSi. The signal amplitude in Figure 5A is equivalent to a 1 cm path length solution of ∼0.6 μM excited RC for this particular sample prepared with a 6 μM RC concentration in the incubation medium. Assuming a surface area to volume ratio of approximately 100 m^2/cm^3 for our porous PSi material (Agarwal, unpublished result), the total surface area in the illuminated active volume in this experiment is estimated to be 90 cm^2. The RC local concentration in the same volume (thickness of PSi = 3 μm) is estimated from the transient absorption change as 1 mM, and assuming monolayer coverage and an average area of the RC of 75 nm^2, we obtain ∼40 cm^2 (almost 50% of the available area) for the surface covered by RC. This can be a lower limit because it assumes that in the PSiMc/RC sample the normally saturating flash is able to excite all RC molecules bound to the porous surface.

Although the signal-to-noise ratio is low because of the relatively small amount of RC and mainly large scattering losses, by comparing the two samples important conclusions can be drawn. When the RC was bound to PSiMc through peptide functionalization, the signal amplitude appeared larger and the exponential analysis resulted in a single decay component with a 27 (±3) ms lifetime. When GTA cross-linker was used, the signal amplitude was about two-thirds that of the peptide sample and the decay kinetics became biphasic with a fast (ca. 50%, 14 (±9) ms) and a slow (50%, 230 (±28) ms) component. The fitting parameters are summarized in Table 1. The lifetime of the fast component in the PSiMc/RC

Table 1. Results of the Decomposition of Exponential Decay Curves Represented in Figure 5[a]

	Q_A sample	Q_B sample	GTA sample	peptide sample
A_{fast} (%)	100	11.0 (±0.2)	49 (±13)	100
τ_{fast} (ms)	107.0 (±0.5)	120 (±3)	14 (±9)	27 (±3)
A_{slow} (%)		89.0 (±0.2)	51 (±6)	
τ_{slow} (ms)		1387 (±2)	230 (±28)	

[a] A_{fast} and A_{slow} are the contributions (in percentage) and τ_{fast} and τ_{slow} are the lifetimes of the fast and slow components, respectively. Q_A and Q_B samples are RCs in buffer (10 mM TRIS, pH 8.0, 100 mM NaCl, 0.03% LDAO) with the Q_B site blocked by the specific inhibitor, terbutryne, or fully reconstituted, respectively. "GTA sample" and "peptide sample" indicate samples in which RCs are bound to PSiMc by GTA or by the specific peptide, respectively. r^2 values of 0.97, 0.60, and 0.62 were obtained for the RC decay kinetics in solution, bound to PSiMc by GTA and by the peptide method, respectively.

system is about a few tens of milliseconds with small variations in the two samples we tested. The same lifetime is 120 (±3) ms in solubilized RC in detergent solution (Figure 5B). The latter lifetime could be measured when the Q_B site was blocked by the specific inhibitor, terbutryne (Figure 5B, Q_B site is blocked), or for the small fraction (5−10%) of the sample in which the quinone pool was reconstituted but the Q_B site remained inactive (Figure 5B, Q_B reconstituted). The lifetime of the slow component is 230 (±28) ms for RC in PSi and 1387 (±2) ms in detergent.

In a control experiment, the absorption change in the RC-GTA adduct in solution was also measured. There was only a small, nonsignificant decrease in the lifetime of the slow component after the GTA cross-linking (τ_{slow} = 1100 ms compared to the 1387 ms reported in Table 1), whereas that of the fast component remained the same. This is in good agreement with earlier results of Noks et al. who found that cross-linking the amino groups of RCs affected the electron-transport kinetics only when the incubations were performed under illumination.[35] The charge recombination kinetics were also in good agreement with the native RCs if another type of

dx.doi.org/10.1021/la301888p | Langmuir 2012, 28, 11866−11873

cross-linker, heterobifunctional *N*-succinimidyl 3-(2-pyridyldithio) propionate, was used.[36]

Although the origin of the two components in PSiMc/RC still remains to be verified by experiment, it is reasonable to assume that the fast and slow components can be assigned to the $P^+Q_A^- \rightarrow PQ_A$ and $P^+Q_B^- \rightarrow PQ_B$ charge recombination processes, respectively. With this assumption, it follows that the interaction of the RC with PSi should substantially accelerate the charge recombination from both quinones to the oxidized BChl special pair.

Following this argument, it appears that the GTA-modified sample shows some Q_B activity whereas in the peptide-modified PSi this component is completely missing. The main difference between the two samples is that the peptide coating provides a hydrophobic environment for the RCs, which is not the case when GTA is used. In the hydrophobic environment, the quinone binding/unbinding equilibrium is shifted to unbinding so that the quinone leaves the Q_B site after subsequent washing of the sample by the buffer during the preparation procedure.

The larger amplitude of the absorption change indicates that the peptide coating provides a more favorable environment for the RC binding (i.e., more RCs are bound to PSiMc). This finding correlates with the larger red shift in the resonance peak position of the reflectivity with the peptide method. The ratio of the $\Delta\lambda_{max}$ values (59/38 = 1.55) and that of the maximum amplitudes of the flash-induced absorption changes (Figure 5A, 0.85/0.5 = 1.7) are almost the same for the two samples. This functionality can be further examined when more turnovers are measured with multiple excitation of the complex.

Multiple Turnover. The pathway and kinetics of the overall electron transfer through the RC in living organisms and in reconstituted systems are coupled to the oxidation of cytochrome c_2 (the native electron donor) on the donor side and to the redox cycle of quinones on the acceptor side of the protein. The RC photocycle involves the continuous turnover of both the cytochromes and the quinones; the oxidized donor and the doubly reduced dihydroquinole (QH_2) are released from the protein and replaced by reduced cytochrome and oxidized quinone from their respective pools.

The direct optical detection of cytochrome photooxidation in the cytochrome cycle is a reliable method of tracking the steps in the RC photocycle.[37,38] Exogenous (such as mammalian) cytochrome *c* can serve as an appropriate electron donor to the RC in in vitro experiments. The oxidation of cytochrome *c* can be followed by the gradual decrease in the absorption at 550 nm after flash excitation. Both the kinetics and the magnitude of the absorption change are strongly dependent on the size (i.e., the redox state) of all components in the pool and the interactions among them.

Indeed, we could measure the decrease in the absorption at 550 nm in the bulk solution which serves as a pool for the cytochrome and quinone supply for the RC when a series of actinic flashes were applied to the PSiMc/RC sample surface. The absorption change indicates that there is an accumulation of oxidized cytochrome *c* in the bulk phase of the reaction mixture due to the RC photochemistry and that the cytochrome oxidation also depends on the UQ-0 concentration. Both the amount of initially oxidized cytochrome per flash and its equilibrium concentration (after about 1 s) depend on the size of the quinone pool. At low quinone concentration, the amplitude of the signal is smaller and there is a decay after every flash. This can be due to the direct redox shuttle between the reduced quinones and oxidized cytochromes in the bulk solution. As demonstrated in Figure 6, the cytochrome oxidation was blocked by terbutryne, which is a competitive

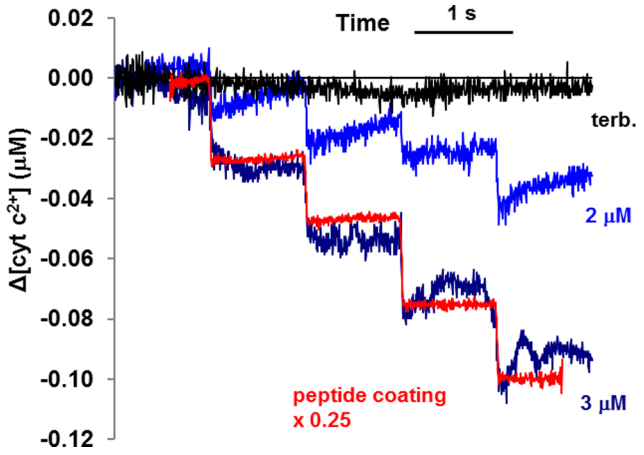

Figure 6. Concentration change in reduced cytochrome *c* (cyt c^{2+}) in the aqueous medium measured at 550 nm after a series of saturating flash excitations when RCs were bound to PSiMc through GTA cross-linking (blue and black) or through peptide coating (red). The reaction mixture contained 12 μM horse heart cytochrome *c* and 2 and 3 μM UQ-0 as indicated. Data obtained in the presence of RC inhibitor terbutryne are also shown. The repetition rate of the flash excitation was 1 Hz.

inhibitor of the electron transport on the acceptor (i.e., the Q_B quinone) side. The reaction kinetics within the RC and those connected to the pools (quinone, cytochrome, and perhaps PSi) are the result of complex equilibria (redox and binding/unbinding) between the components, which can be affected by terbutryne. These complex redox and binding equilibria, specifically close to the surface of PSi, could be the subject of further studies.

It was found earlier that the peptide coating provides a better environment for binding proteins to PSiMc. Both the number of proteins bound to PSi and their functionalities were enhanced.[17] Figure 6 shows that the RC binding and action are also more favorable when RC is bound through the peptide to PSiMc. When the samples were prepared and the measurement was carried out under the same conditions, 4 times more oxidized cytochrome was produced when the peptide coating was applied.

Hence, after binding the RC to PSi the Q_B site is still accessible either to quinones or to the inhibitor (at least to UQ-0 and to terbutryne), and the RC can also be reduced by exogenous cytochrome *c*, whose site of interaction may or may not be the native donor site.

■ CONCLUSIONS

For the first time, the fabrication and preliminary characterization of a hybrid system with a photoactive bionanocomposite, made up of photosynthetic reaction center protein and a porous silicon photonic structure, have been reported. The *Rhodobacter sphaeroides* reaction center protein was bound to porous silicon by the GTA cross-linker after silanization and through peptide coating. A successful infiltration of the RC protein into the PSi photonic structure with the retention of its photochemical activity has been demonstrated. Light-induced charge recombination showed highly biphasic character in GTA and monophasic character in the peptide coating, but the

reconstitution of the Q_B site could be demonstrated by the multiple turnover experiment. After the reconstitution of the donor and acceptor sites, the RC photocycle was also restored and the accessibility of the secondary quinone site to exchangeable cofactors was not blocked in the PSi matrix.

Several properties of this bionanocomposite are of special interest: (a) The protein bound to PSi can be activated by light, and there is a charge separation after light activation. The generated dipole might interfere with the photonic properties of the PSiMc and interact electronically with the silicon substrate. (b) Large (ca. 100 kDa) and (c) highly hydrophobic protein is bound to the pores, which was not published until now in the literature. (d) It is foreseen that the combination of the special characteristics of the PSi and RC offers unique, new generation application possibilities.

MATERIALS AND METHODS

Sample Preparation. *Rb. sphaeroides* R-26 cells were grown photoheterotrophically.[39,40] RCs were prepared by LDAO (*N*,*N*-dimethyldodecylamine-*N*-oxide, Fluka) solubilization and purified by ammonium sulfate precipitation, followed by DEAE Sephacel (Sigma) anion-exchange chromatography.[41]

PSiMc-s were prepared by a wet electrochemical etching process using highly boron-doped p-type silicon wafers (thickness 500−550 μm) with a 0.002−0.004 ohm cm specific resistivity and with a crystallographic orientation of (100). The electrolyte consisted of hydrofluoric acid (48 wt %), ethanol (98%), and glycerol (98%) in a volumetric ratio of 3:7:1.[13,31] The microcavity structures were fabricated with the configuration of $(HL)_{x5}HH(LH)_{x5}$ where H and L represent high and low porosity layers, respectively. Because the optical thickness of each layer was kept at $^{\lambda}/_{4}$ (with λ = 700 nm), the presence of two successive layers of high porosity in the middle creates a cavity mode with an optical thickness of $^{\lambda}/_{2}$. To ensure good macromolecular penetration, the multilayers were prepared with the first layer as a high porosity one. The samples were thermally oxidized at 900 °C for 3 min.

RCs were bound to PSiMc in two different ways. The first method involved a three-step conjugation protocol. The PSi surface was first functionalized using the amine group of 3-aminopropyl-triethoxysilane (APTES), followed by the binding of glutaraldehyde (GTA) as an amine-targeted homobifunctional cross-linker. Finally, the RC was bound to GTA through its surface-accessible lysine side chains.[18] The thermally oxidized PSiMc samples were incubated for 2 h in 5% APTES (Aldrich) diluted in toluene and then rinsed with a toluene/ethanol mixture (1:1) and ethanol. The samples were dried under a stream of N_2 and baked at 100 °C for 15 min. The activation of the amine group was performed by incubating the silanized-PSiMc samples in 2.5% GTA (Sigma) in PBS buffer at pH 7.2 for 20 min, followed by rinsing with PBS and drying under a stream of N_2. In the second method, the RC was bound to PSi through a 12-mer peptide (SPGLSLVSHMQT) previously elaborated as a specific linker for p^+-Si surfaces.[17] Briefly, the deoxidized (by HCl), freshly etched PSi sample was exposed to the peptide solution (20 μM in PBST) for 2 h, the unbound peptide was washed away with PBST, and the samples were dried under N_2. To bind the RC, drops of the protein solution (in 10 mM TRIS, 0.03% LDAO, pH 8.0) were placed on the sample surface for 90 min, followed by washing with PBS buffer and drying under a stream of N_2.

Scanning Electron Microscopy. Scanning electron microscopy (SEM) was performed with a Hitachi S-4700 type II FE-SEM equipped with a cold field emission gun operating in the range of 5−15 kV. The samples were mounted on a conductive carbon tape and sputter coated with a thin Au/Pd layer in an Ar atmosphere prior to the measurement. To characterize the element distribution within the PSi structure, energy-dispersive X-ray analyses (EDX) were also performed using a RÖNTEC XFlash Detector 3001 with a silicon drift detector (SDD).

Specular Reflectometry. Reflectivity spectra were recorded with a Bruker 66 V Fourier Transform Infrared spectrometer using the Bruker A 510, 11° specular reflection unit. The PSi samples were illuminated with the tungsten source, and the reflected beam was detected with the silicon diode detector. The resulting spectrum captured in the range of 25 000−9000 cm^{-1} after each modification step of the porous silicon was the average of 100 scans and had a spectral resolution of 2 cm^{-1}.[17,18]

Optical Spectroscopy. Flash-induced absorption changes were measured at 860 nm by the single-beam kinetic spectrophotometer of local design described earlier, with a geometrical modification to allow its operation in reflection mode instead of transmission mode.[38] The measuring light beam was incident on the surface of the RC-functionalized PSiMc sample at 45° and reflected toward the photomultiplier tube detector (Hamamatsu R928). For activation, the beam of a Xe flash lamp (EG&G FX200, $t_{1/2}$ = 8.5 μs) was projected perpendicularly on the sample surface through an optical fiber. At 860 nm, the redox state of the P/P^+ couple can be monitored without a substantial contribution by the other cofactors of the RC.

The oxidation of horse heart cytochrome *c* (Sigma) by RCs bound to PSi was measured at 550 nm in transmission mode. The PSiMc sample containing the bound RCs was placed in a 1 cm × 1 cm spectroscopic cuvette containing buffer solution (10 mM TRIS, 100 mM NaCl, 0.03% LDAO, pH 8.0, and reagents as indicated in the legend of Figure 6) next to its rear wall facing the Xe flash beam, thereby avoiding the perpendicular measuring light beam. A series of actinic Xe flashes were applied with a repetition rate of 1 Hz. The amount of cytochrome *c* oxidized by the RCs was determined using the difference in the extinction coefficient $\varepsilon_{red} - \varepsilon_{ox}$ = 21.1 ± 0.4 mM^{-1} cm^{-1}.[42] Cytochrome *c* was reduced by ascorbate before the experiments. For the reconstitution of the quinone electron-acceptor side, water-soluble UQ-0 (2,3-methoxy-5-methyl-1,4-ubiquinone, Sigma) was used.

AUTHOR INFORMATION

Corresponding Author

*E-mail: csilla.gergely@univ-montp2.fr.

Notes

The authors declare no competing financial interest.

ACKNOWLEDGMENTS

This work was supported by grants from the bilateral agreement of MTA (Hungary) and CONACYT (Mexico) (project no. 122017); the Swiss National Science Foundation (IZ73Z0_128037/1); the Swiss Contribution (SH/7/2/20); and the Hungarian-French Intergovernmental S&T Cooperation Programme (project nos. 10-1-2011-0735 (Hungary), 25030RB (France), and TÁMOP-4.2.1/B-10/1-2010-0012). Thanks are due to the French Governement fellowship (Cotutelle) provided to K.H. for her studies at Montpellier.

ABBREVIATIONS

$(BChl)_2$, bacteriochlorophyll dimer; BPheo, bacteriopheophytin; EDX, energy-dispersive X-ray analysis; FSM, folded-sheet mesoporous silica material; GOX, glucose oxidase; GTA, glutaraldehyde; APTES, 3-aminopropyl-triethoxysilane; LHC, light-harvesting pigment protein complex; MPS, mesoporous silica material; PSi, porous silicon; PSiMc, porous silicon microcavity; Q_A, primary quinone; Q_B, secondary quinone; RC, photosynthetic reaction center; SBA, Santa Barbara amorphous porous silica material; SEM, scanning electron microscopy; PBST, phosphate-buffered saline solution containing 0.1% TWEEN-20

REFERENCES

(1) Shoseyov, O.; Levy, I. *Nanobiotechnology: Bioinspired Devices and Materials of the Future*; Humana Press. Inc.: Totowa, NJ, 2008.

(2) Darder, M.; Aranda, P.; Ruiz- Hitzky, E. Bionanocomposites: A New Concept of Ecological, Bioinspired, and Functional Hybrid Materials. *Adv. Mater.* **2007**, *19*, 1309−1319.

(3) Giardi, M. T.; Pace, E. Photosynthetic Proteins for Technological Applications. *Trends. Biotechnol.* **2005**, *23*, 257−263.

(4) Ormos, P.; Fábián, L.; Oroszi, L.; Wolff, E. K.; Ramsden, J. J.; Dér, A. Protein-Based Integrated Optical Switching and Modulation. *Appl. Phys. Lett.* **2002**, *80*, 4060−4062.

(5) Aroutiounian, V. M.; Martirosyan, K. S.; Hovhannisyan, A. S.; Soukiassian, P. G. Use of Porous Silicon for Double- and Triple-Layer Antireflection Coatings in Silicon Photovoltaic Converters. *J. Contemp. Phys. (Arm. Acad. Sci.)* **2008**, *43*, 72−76.

(6) Xua, J.; Bhattacharya, P.; Váró, G. Monolithically Integrated Bacteriorhodopsin/Semiconductor Opto-Electronic Integrated Circuit for a Bio-Photoreceiver. *Biosens. Bioelectron.* **2004**, *19*, 885−892.

(7) Wraight, C. A.; Clayton, R. The Absolute Quantum Efficiency of Bacteriochlorofill Photooxidation in Reaction Centres of Rhodopseudomonas Sphaeroides. *Biochem. Biophys. Acta* **1974**, *333*, 246−260.

(8) Meunier, C. F.; Rooke, J. C.; Hajdu, K.; Cutsem, P. V.; Cambier, P.; Leonard, A.; Su, B. L. Insight into Cellular Response of Plant Cells Confined within Silica-Based Matrices. *Langmuir* **2010**, *26*, 6568−6575.

(9) Fukushima, Y.; Inagaki, S. Nano-Scale Structure Control of Mesoporous Silica. *Mater. Sci. Eng., A* **1996**, *217/218*, 116−118.

(10) Oda, I.; Iwaki, M.; Fujita, D.; Tsutsui, Y.; Ishizaka, S.; Dewa, M.; Nango, M.; Kajino, T.; Fukushima, Y.; Itoh, S. Photosynthetic Electron Transfer from Reaction Center Pigment-Protein Complex in Silica Nanopores. *Langmuir* **2010**, *26*, 13399−13406.

(11) Noji, T.; Kamidaki, C.; Kawakami, K.; Shen, J. R.; Kajino, T.; Fukushima, Y.; Sekitoh, T.; Itoh, S. Photosynthetic Oxygen Evolution in Mesoporous Silica Material: Adsorption of Photosystem II Reaction Center Complex into 23 nm Nanopores in SBA. *Langmuir* **2011**, *27*, 705−713.

(12) Oda, I.; Hirata, K.; Watanabe, S.; Shibata, Y.; Kajino, T.; Fukushima, Y.; Iwai, S.; Itoh, S. Function of Membrane Protein in Silica Nanopores: Incorporation of Photosynthetic Light-Harvesting Protein LH2 into FSM. *J. Phys. Chem. B* **2006**, *110*, 1114−1120.

(13) Agarwal, V.; del Río, J. A. Tailoring the Photonic Band Gap of a Porous Silicon Dielectric Mirror. *Appl. Phys. Lett.* **2003**, *82*, 1512−1514.

(14) Estevez, J. O.; Arriaga, J.; Méndez Blas, A.; Agarwal, V. Enlargement of Omnidirectional Photonic Bandgap in Porous Silicon Dielectric Mirrors with a Gaussian Profile Refractive Index. *Appl. Phys. Lett.* **2009**, *94*, 061914 DOI: .

(15) Martin, M.; Palestino, G.; Cloitre, T.; Agarwal, V.; Zimanyi, L.; Gergely, C. Three-Dimensional Spatial Resolution of the Nonlinear Photoemission from Biofunctionalized Porous Silicon Microcavity. *Appl. Phys. Lett.* **2009**, *94*, 223313.

(16) Thompson, C. M.; Nieuwoudt, M.; Ruminski, A. M.; Sailor, M. J.; Miskelly, G. M. Electrochemical Preparation of Pore Wall Modification Gradients Across Thin Porous Silicon Layers. *Langmuir* **2010**, *26*, 7598−7603.

(17) Estephan, E.; Saab, M.-B.; Agarwal, V.; Cuisinier, F. J. G.; Larroque, C.; Gergely, C. Peptides for the Biofunctionalization of Silicon for Use in Optical Sensing with Porous Silicon Microcavities. *Adv. Funct. Mater.* **2011**, *21*, 2003−2011.

(18) Palestino, G.; Legros, R.; Agarwal, V.; Pérez, E.; Gergely, C. Functionalization of Nanostructured Porous Silicon Microcavities for Glucose Oxidase Detection. *Sens. Actuators, B* **2008**, *135*, 27−34.

(19) Xiao, L.; Gu, L.; Howell, S. B.; Sailor, M. J. Porous Silicon Nanoparticle Photosensitizers for Singlet Oxygen and Their Phototoxicity against Cancer Cells. *ACS Nano* **2011**, *5*, 3651−3659.

(20) Wu, E. C.; Andrew, J. S.; Buyanin, A.; Kinsella, J. M.; Sailor, M. J. Suitability of Porous Silicon Microparticles for the Long-Term Delivery of Redox-Active Therapeutics. *Chem. Commun.* **2011**, *47*, 5699−5701.

(21) Kilian, K. A.; Böcking, T.; Ilyas, S.; Gaus, K.; Jessup, W.; Gal, M.; Gooding, J. J. Forming Antifouling Organic Multilayers on Porous Silicon Rugate Filters towards in Vivo/Ex Vivo Biophotonic Devices. *Adv. Funct. Mater.* **2007**, *17*, 2884−2890, DOI: .

(22) Orosco, M. M.; Pacholski, C.; Miskelly, G. M.; Sailor, J. Protein-Coated Porous-Silicon Photonic Crystals for Amplified Optical Detection of Protease Activity. *Adv. Mater.* **2006**, *18*, 1393−1396.

(23) Allen, J. P.; Williams, J. C. Photosynthetic Reaction Centers. *FEBS Lett.* **1998**, *438*, 5−9.

(24) Paddock, M. L.; Feher, G.; Okamura, M. Y. Proton Transfer Pathways and Mechanism in Bacterial Reaction Centers. *FEBS Lett.* **2003**, *555*, 45−50.

(25) Wraight, C. A. Proton and Electron in the Acceptor Quinone Complex of Photosynthetic Reaction Centers from Rhodobacter Sphaeroides. *Front. Biosci.* **2004**, *9*, 309−337.

(26) Nagy, L.; Hajdu, K.; Fisher, B.; Hernádi, K.; Nagy, K.; Vincze, J. Photosynthetic Reaction Centres − From Basic Research to Application Possibilities. *Not. Sci. Biol.* **2010**, *2*, 7−13.

(27) Hajdu, K.; Szabó, T.; Magyar, M.; Bencsik, G.; Németh, Z.; Nagy, K.; Forró, L.; Váró, Gy.; Hernádi, K.; Nagy, L. Photosynthetic Reaction Center Protein in Nanostructures. *Phys. Status Solidi B* **2011**, *248*, 2700−2703, DOI: .

(28) Lu, Y.; Xu, Y.; Liu, B.; Kong, J. Photosynthetic Reaction Centre Functionalized Nano-composite Films: Effective Strategies for Probing and Exploiting the Photo-Induced Electron Transfer of Photosensitive Membrane Protein. *Biosens. Bioelectron.* **2007**, *22*, 1173−1185.

(29) Dorogi, M.; Bálint, Z.; Mikó, C.; Vileno, B.; Milas, M.; Hernádi, K.; Forró, L.; Váró, G.; Nagy, L. Stabilization Effect of Single Walled Carbon Nanotubes on the Functioning of Photosynthetic Reaction Centers. *J. Phys. Chem. B* **2006**, *110*, 21473−21479.

(30) Ohmori, H.; Nagy, L.; Dorogi, M.; Terazima, M. Charge Stabilization in Reaction Center Protein Investigated by Optical Heterodyne Detected Transient Grating Spectroscopy. *Eur. Biophys. J. (Biophys. Lett.)* **2008**, *37*, 1167−1174.

(31) Agarwal, V.; del Río, J. A.; Zamfirescu, G. M.; Kavokin, A.; Coquillat, D.; Scalbert, D.; Vladimirova, M.; Gil, B. Photon Bloch Oscillations in Porous Silicon Optical Superlattices. *Phys. Rev. Lett.* **2004**, *92*, 097401.

(32) Gerencsér, L.; Laczkó, G.; Maróti, P. Unbinding of Oxidized Cytochrome c from Photosynthetic Reaction Center of Rhodobacter sphaeroides is the Bottleneck of Fast Turnover. *Biochemistry* **1999**, *38*, 16866−1875.

(33) Saab, M. B.; Estephan, E.; Cloitre, T.; Larroque, C.; Gergely, C. Peptide Route Functionalization of ZnSe Crystals Preserves Activity and Structure of Proteins while Adsorption. *J. Phys. Chem. C* **2010**, *114*, 18509−18515.

(34) Straley, S. C.; Parson, W. W.; Mauzerall, D. C.; Clayton, R. K. Pigment Content and Molar Extinction Coefficients of Photochemical Reaction Centers from Rhodopseudomonas Spheroides. *Biochim. Biophys. Acta* **1973**, *305*, 597−609.

(35) Noks, P. P.; Lukashev, E. P.; Kononenko, A. A.; Venediktov, P. S.; Rubin, A. B. Possible Role of Macromolecular Components in the Functioning of Photosynthetic Reaction Centers of Purple Bacteria. *Mol. Biol. (Moscow)* **1977**, *11*, 1090−1099.

(36) Ueno, T.; Hirata, Y.; Hara, M.; Arai, T.; Sato, A.; Miyake, J.; Fujii, T. Formation of Cross-Linked Complex of Photosynthetic Reaction Center and Horse Heart Cytochrome c: An Approach for Molecular Organization with Cross-Linkage. *Mater. Sci. Eng. C* **1995**, *3*, 1−6.

(37) Kleinfeld, D.; Okaamura, M. Y.; Feher, G. Electron Transfer in Reaction Centers of Rhosopseudomonas Sphaeroides. I. Determination of the Charge Recombination Pathway of $D^+Q_AQ_B^-$ and Free Energy and Kinetic Relations Between $Q_A^-Q_B$ and $Q_AQ_B^-$. *Biochem. Biophys. Acta* **1984**, *766*, 126−140.

(38) Osváth, S.; Maróti, P. Coupling of Cytochrome and Quinone Turnovers in the Photocycle of Reaction Centers from the Photosynthetic Bacterium Rhodobacter Sphaeroides. *Biophys. J.* **1996**, *73*, 972−982.

(39) Ormerod, J. G.; Ormerod, K. S.; Gest. Light-Dependent Utilization of Organic Compounds and Photoproduction of Molecular Hidrogen by Photosynthetic Bacteria; Relationships with Nitrogen Metabolism. *Arch. Biochem. Biophys.* **1961**, *94*, 449−463.
(40) Nagy, L.; Puskás, Á.; Tandori, J.; Droppa, M.; Horváth, G. Effect of DCMU on Photosynthetic Purple Bacteria. *Photosynthetica* **1991**, *25*, 167−171.
(41) Tandori, J.; Nagy, L.; Puskas, A.; Droppa, M.; Horvath, G.; Maróti, P. The Ile^{L229} –> Met Mutation Impairs the Quinone Binding to the Q_B-Pocket in Reaction Centers of Rhodobacter Sphaeroides. *Photosynth. Res.* **1995**, *45*, 135−146.
(42) Van Gelder, B. F.; Slater, E. C. The Extinction Coefficient of Cytochrome c. *Biochim. Biophys. Acta* **1962**, *58*, 593−595.